Materials Today Bio 26 (2024) 101049

Contents lists available at ScienceDirect

Materials Today Bio

journal homepage: www.journals.elsevier.com/materials-today-bio

Zwitterionic polymer-dexamethasone conjugates penetrate and protect cartilage from inflammation

Patrick Weber, Maryam Asadikorayem, František Surman, Marcy Zenobi-Wong *

Tissue Engineering + Biofabrication Laboratory, Department of Health Sciences and Technology, ETH Zürich, Otto-Stern-Weg 7, 8093, Zürich, Switzerland

ARTICLE INFO

Keywords:
Zwitterionic
Dexamethasone
Polymer-drug conjugate
Cartilage
Sustained release

ABSTRACT

Improving the pharmacokinetics of intra-articularly injected therapeutics is a major challenge in treating joint disease. Small molecules and biologics are often cleared from the joint within hours, which greatly reduces their therapeutic efficacy. Furthermore, they are often injected at high doses, which can lead to local cytotoxicity and systemic side effects. In this study, we present modular polymer-drug conjugates of zwitterionic poly(carboxybetaine acrylamide) (pCBAA) and the anti-inflammatory glucocorticoid dexamethasone (DEX) to create cartilage-targeted carriers with slow-release kinetics. pCBAA polymers showed excellent cartilage penetration (full thickness in 1 h) and retention (>50 % after 2 weeks of washing). DEX was loaded onto the pCBAA polymer by employing two different DEX-bearing comonomers to produce pCBAA-co-DEX conjugates with different release kinetics. The slow-releasing conjugate showed zero-order release kinetics in PBS over 70 days. The conjugates elicited no oxidative stress on chondrocytes compared to dose-matched free DEX and protected bovine cartilage explants from the inflammatory response after treatment with IL-1β. By combining cartilage targeting and sustained drug release properties, the pCBAA-co-DEX conjugates solve many issues of today's intra-articular therapeutics, which could ultimately enable better long-term clinical outcomes with fewer side effects.

1. Introduction

Degenerative joint disease is one of the most common conditions in humans, affecting more than a third of individuals older than 65 years [1]. Despite its high prevalence and associated socio-economic costs, we still lack effective pharmacological treatment options to achieve a satisfactory outcome in the long run. One problem is the poor pharmacokinetic profile of intra-articularly (IA) injected therapeutics. Due to the permeability of the joint capsule, therapeutics are rapidly cleared from the joint within hours (small molecules) [2,3] to a few days (high-molecular weight hyaluronic acid) [4,5]. This not only reduces the duration of the therapeutic effect but also creates the risk of systemic side effects as the drug leaves the joint cavity and enters the blood stream [2,6].

IA glucocorticoids (GCs) are probably the most frequently discussed class of therapeutics in that context: GCs are powerful, broad-spectrum anti-inflammatory drugs derived from natural cortisone that have been in clinical use to treat joint disease since the 1950s [7]. Though IA GCs continue to be used and recommended for the treatment of knee osteoarthritis (OA) [8–11], their therapeutic efficacy is controversial, due to several clinical studies reporting harmful effects of in the long run [12–15]. For example, *McAlindon* et al. reported that after two years, patients receiving repeated IA GCs showed decreased cartilage thickness as well as increased joint pain compared to the control subjects [15]. Furthermore, several *in vitro* studies have linked GCs to apoptosis [16,17], decreased extracellular matrix (ECM) synthesis [18,19] and increased production of reactive oxygen species (ROS) [17,20] in chondrocytes.

These findings stand in stark contrast to a large body of literature demonstrating not just anti-inflammatory but also potential disease-modifying effects of GCs in the context of OA. For example, *Lu* et al. showed that sustained treatment of cartilage explants with low-dose GCs

Abbreviations: APTAC, (3-acrylamidopropyl)trimethylammonium; CBAA, Carboxybetaine acrylamide; C2Pep, Acrylamide-Ahx-WYRGRL collagen II-binding peptide; DEX, Dexamethasone; DEX-MAES, dexamethasone-mono-2-(methacryloyloxy)ethyl succinate; DEX-MAHAc, dexamethasone-6-methacrylamidohexanoic acid; DMA, dopamine methacrylate; HPMA, *N*-(2- hydroxypropyl)methacrylamide; PEGMA, Polyethylene glycol methacrylate; PCMA, 2-Methacryloyloxyethyl phosphorylcholine.

* Corresponding author.
E-mail addresses: patrick.weber@hest.ethz.ch (P. Weber), maryam.asadikorayem@hest.ethz.ch (M. Asadikorayem), frsurman@gmail.com (F. Surman), marcy.zenobi@hest.ethz.ch (M. Zenobi-Wong).

https://doi.org/10.1016/j.mtbio.2024.101049
Received 26 January 2024; Received in revised form 4 April 2024; Accepted 8 April 2024
Available online 10 April 2024

completely protected them from both inflammation- and trauma-induced ECM degradation [21]. Furthermore, GC treatment completely preserved ECM synthesis levels compared to the untreated control. In a similar study, *Li* et al. found that, in addition to decreased loss of cartilage ECM, GC-treated explants actually showed increased cell viability compared to the inflamed controls [22]. In both of these examples, the GC was administered continuously over the entire experiment and at concentrations up to 5 orders of magnitude below the clinical concentration [13]. This implies that the problem does not lie with the choice of drug but rather with the kinetics and the concentration at which it is being delivered – a conclusion that may help explain not only the controversy around IA GCs but also the failure of many other OA therapeutics in clinical trials [23,24].

Consequently, we have seen the development of many IA drug delivery vehicles in recent years, including hydrogel microparticles [25,26], hydrogel nanoparticles [27,28], *in situ*-forming hydrogels [29], liposomes [30,31] and polymer-drug conjugates [32–35]. Generally, these platforms achieve prolonged joint retention by either exceeding the size of the capillary fenestrations in the synovial membrane [36] or by being actively targeted towards one or several tissues within the joint cavity [37]. To achieve active targeting to cartilage, cationic carriers are a popular choice due to the anionic glycosaminoglycans (GAGs) in the cartilage ECM [38]. For GCs specifically, *Bajpayee* et al. and *Formica* et al. produced conjugates of dexamethasone (DEX) with the cationic protein avidin [39,40] and the cationic polysaccharide chitosan [32] respectively, to improve cartilage uptake and achieve sustained drug release. Though both systems were able to reduce inflammation-induced ECM degradation, the pursued post-functionalization strategies are highly optimized for the specific carrier which limits the overall versatility and tailorability of these approaches. For avidin-DEX specifically, the choice of the avidin-biotin interaction for DEX anchoring also greatly limits drug loading to only 4 DEX molecules per construct. The post-functionalization approach of chitosan-DEX on the other hand offers only poor control over drug loading resulting in large batch-to-batch variability. To increase control and tailorability, *Zhao* et al. synthesized a polymerizable DEX comonomer which could be polymerized with N-(2- hydroxypropyl)methacrylamide (HPMA) to create pHPMA-DEX with a precisely controllable degree of substitution [34]. These copolymers reached IA retention times *in vivo* of more than one month, as they formed macroscopic, phase-transitioned hydrogels at physiological temperature. However, they did not penetrate cartilage, thus delivering GCs in an untargeted way. In this study, we combine the advantages of both approaches by creating highly tailorable polymer-drug conjugates through copolymerization that are targeted towards the cartilage ECM and enable a slow and continuous delivery of GCs (Fig. 1).

Our platform comprises three principal components that all carry either a (meth)acrylate or (meth)acrylamide group and can be copolymerized at user-defined ratios using standard "one-pot" free radical polymerization. The largest mole-fraction within our polymers is made up of zwitterionic (ZI) monomers, namely carboxybetaine acrylamide (CBAA) or phosphorylcholine methacrylate (PCMA). Zwitterionic polymers carry equal numbers of anionic and cationic charges in close spatial proximity, leading to extremely high levels of hydration and therefore excellent non-fouling properties [41]. Though these materials are non-biodegradable they have shown excellent biocompatibility *in vivo* [42–44]. In addition, due to their very weak interaction with any surrounding (macro)molecules, they have been found to penetrate well into tumor tissue [45,46] – a property that should also translate to cartilage. To not only penetrate cartilage but also to be retained over prolonged periods of time, three different targeting comonomers were introduced: Cationic (3-acrylamidopropyl)trimethylammonium (APTAC) to target the negatively charged GAGs, the hexapeptide WYRGRL (C2Pep) to bind to collagen II [47], the other main component of cartilage ECM, and dopamine methacrylamide (DMA) to non-specifically adhere to the tissue via hydrogen bonds [48]. Finally, fast and slow release DEX-bearing comonomers (DEX-mono-2-(methacryloyloxy)ethyl succinate (DEX-MAES) and DEX-6-methacrylamidohexanoic acid (DEX-MAHAc)) were synthesized that allow for sustained drug release through passive hydrolysis.

Exploiting the modular nature of our platform, we performed a screening to arrive at a conjugate that (1) showed full thickness cartilage

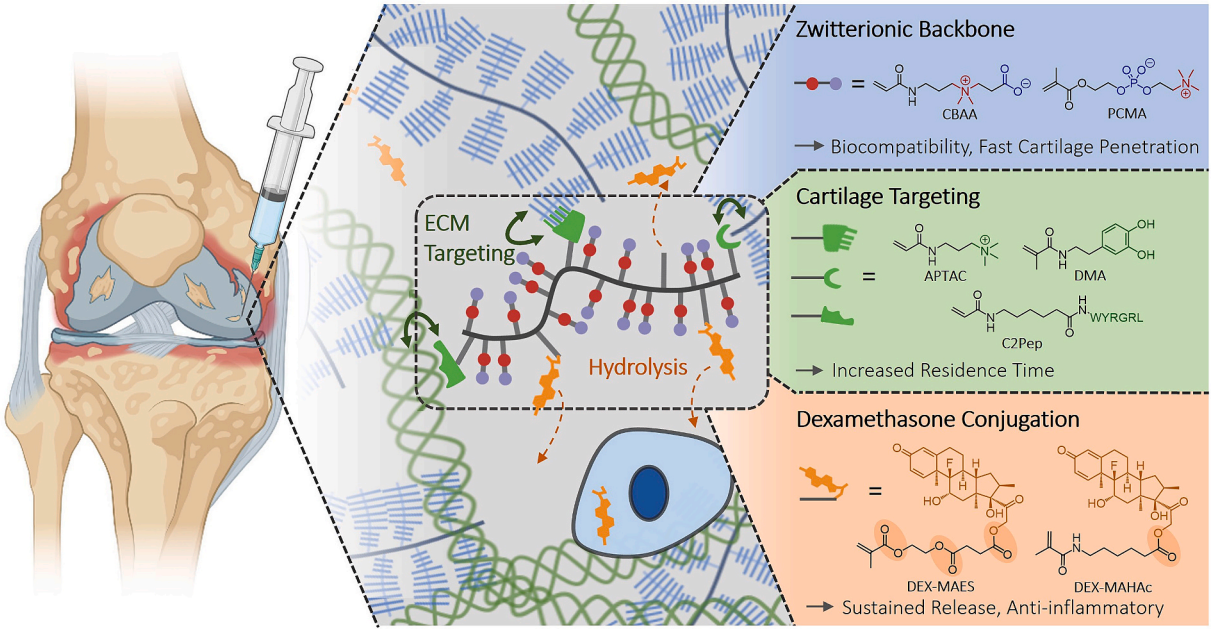

Fig. 1. Project overview: Modular polymer-drug conjugates were produced to achieve cartilage-targeted, sustained release of anti-inflammatory drugs. The system consists of three components that can be combined at user-defined ratios to convey specific properties to the conjugate. Hydrolytic release kinetics can be adapted by choosing DEX-comonomers with different numbers of esters in the linker. CBAA: (3-Acryloylaminopropyl)-(2-carboxy-ethyl)-dimethyl-ammonium, PCMA: 2-Methacryloyloxyethyl phosphorylcholine, APTAC: (3-acrylamidopropyl)trimethylammonium, DMA: dopamine methacrylate, C2Pep: Acrylamide-Ahx-WYRGRL collagen II-binding peptide, DEX-MAES: dexamethasone-mono-2-(methacryloyloxy)ethyl succinate, DEX-MAHAc: dexamethasone-6-methacrylamidohexanoic acid. Figure created with BioRender.

penetration within 1 h, (2) was retained in cartilage for more than 2 weeks, (3) displayed zero-order release kinetics in PBS over more than 2 months and ultimately (4) protected cartilage from IL-1β-induced inflammation.

2. Materials and methods

2.1. Chemicals

Unless otherwise stated, all chemicals were purchased from Sigma-Aldrich (Buchs, CH).

2.2. Monomer synthesis

2.2.1. Carboxybetaine acrylamide (CBAA)

CBAA (IUPAC: (3-Acryloylaminopropyl)-(2-carboxy-ethyl)-dimethyl-ammonium) was synthesized as previously reported [49]: 14.9 g freshly distilled N-[3-(Dimethylamino)propyl] acrylamide (95 mmol, TCI Chemicals, Tokyo, JPN) was dissolved in 100 mL of dry THF and cooled to −10 °C. 9.6 g of β-propiolactone (8.4 mL, 134 mmol, 1.4 eq., Acros Organics, Waltham, USA) dissolved in 25 mL of dry THF were added dropwise over 40 min. The reaction mixture was left stirring for another 4 h before the flask was kept statically at −20 °C overnight. The white precipitate was filtered off on a fritted-glass filter (S4 porosity) and washed with three volumes of cold diethylether to yield 13 g of CBAA (57 mmol, 60 % yield). ^{1}H NMR (Fig. S1, Bruker 400 MHz in D_2O): δ (ppm) 6.32 (dd, 1H, CHH═C*H*), 6.2 (dd, 1H, CH*H*═CH), 5.87 (dd, 1H, C*H*H═CH), 3.66 (t, 2H, N–C*H*$_2$–CH$_2$–COO), 3.48 (m, 4H, NH–C*H*$_2$–CH$_2$–C*H*$_2$), 3.17 (s, 6H, N-(C*H*$_3$)$_2$), 2.75 (t, 2H, C*H*$_2$–COO). 1.98 (dt, 2H, NH–CH$_2$–C*H*$_2$–CH$_2$)

2.2.2. Dopamine methacrylamide (DMA)

DMA was synthesized as previously reported [48]: 4.0 g $Na_2B_4O_7$ (10.5 mmol, 1 eq.) and 1.6 g $NaHCO_3$ (19.0 mmol, 1.8 eq.) were dissolved in dH_2O and purged with N_2 for 20 min 2.0 g dopamine-HCl (10.5 mmol) were dissolved in this aqueous solution, to which then 1.9 mL methacrylate anhydride (11.6 mmol, 1.2 eq.) in 10 mL of dry THF was added dropwise. The pH of the reaction mixture was kept above 8 with aq. 1 M NaOH. The mixture was stirred overnight at room temperature with N_2 bubbling. The reaction mixture was acidified (pH < 2) with conc. HCl and washed four times with ethyl acetate. The combined organic phases were dried over $MgSO_4$ and the solution concentrated under reduced pressure to 10 mL. Precipitation of the product was triggered by the addition of 100 mL of n-hexane under vigorous stirring. The mixture was kept at 4 °C overnight, the light brown precipitate filtered off on a fritted-glass filter (S4 porosity) and washed with 3 volumes of n-hexane to yield 1.95 g of DMA (8.8 mmol, 84 % yield). ^{1}H NMR (Fig. S2, Bruker 400 MHz in DMSO-d_6): δ (ppm) 8.78–8.57 (d, 2H, C_6H*H*$_2$(O*H*)$_2$), 7.92 (t, 1H, C_6H_3(OH)$_2$–CH$_2$–CH$_2$(N*H*)–C(=O)), 6.66–6.55 (m, 2H, C_6H*H*$_2$(OH)$_2$), 6.43 (dd, 1H, C_6H_2*H*(OH)$_2$), 5.62 (s, 1H, C(=O)–C(-CH$_3$)═C*H*H), 5.30 (s, 1H, C(=O)–C(-CH$_3$)═CH*H*), 3.23 (m, 2H, C_6H_3(OH)$_2$–CH$_2$–C*H*$_2$(NH)–C(=O)), 2.55 (t, 2H, C_6H_3(OH)$_2$–C*H*$_2$–CH$_2$(NH)–C(=O)), 1.84 (s, 3H, C(=O)–C(-C*H*$_3$)═CH$_2$)

2.2.3. Acrylamide-Ahx-WYRGRL collagen II-binding peptide (C2Pep)

The collagen II binding peptide sequence was based on a study by *Rothenfluh* et al. that identified the WYRGRL hexapeptide as a specific collagen II binder [47]. To increase the exposure and flexibility of the peptide once incorporated into pCBAA, an aminocaproic acid (Ahx) linker was added at the N-terminus. The peptide was synthesized using standard Fmoc solid phase chemistry on a Prelude X peptide synthesizer (Protein Technologies, Inc., Tucson, USA) at 500 μmol scale on a Rink Amide MBHA Resin (HL, 0.69 mmol/g, Gyros Protein Technologies, Uppsala, SWE). Each coupling step comprised a 2 × 1 min Fmoc deprotection with 20 % v/v piperidine in DMF, followed by addition of the amino acid (1 mmol, 2 eq.), 0.4 M *N,N,N′,N′*-tetramethyl-*O*-(1H-benzotriazol-1-yl) uronium hexafluorophosphate and 0.4 M *N*-methylmorpholine in DMF twice for 5 min. After each coupling, the resin was washed with DMF 3 x 30s. After the final Ahx coupling, the resin-bound peptides were suspended in 15 mL of dry DCM. Triethylamine (6 mmol, 12 eq.) and acryloyl chloride (4.5 mmol, 9 eq.) were added and the reaction mixture stirred on ice overnight. The resin was filtered off and washed 3 times with MeCN and the peptides cleaved off in 4 % v/v TIPS and 4 % dH_2O in trifluoroacetic acid for 1 h under shaking. The peptides were precipitated with 250 mL chilled ether, placed on ice for 20 min, centrifuged (4000×*g*, 10 min, 4 °C), the ether decanted and the pellet air-dried overnight. The pellet was resuspended in 40 mL of 10 % v/v MeCN in dH_2O, the resin filtered off, the peptide purified with preparative HPLC (Agilent Prep, 100 Å C18, 50 × 250 mm, 10 μm, Agilent Technologies, Santa Clara, USA) and the combined product fractions lyophilized to isolate the pure Acrylamide-Ahx-WYRGRL peptide as a fluffy white solid (294 mg, 290 μmol, 58 % yield). LC-MS (Fig. S3, ESI, +, *m/z*): found: 1016.8 theoretical: 1015.6.

2.2.4. Dexamethasone-mono-2-(methacryloyloxy)ethyl succinate (DEX-MAES)

500 mg of Dexamethasone (1.28 mmol, ABCR, Karlsruhe, GER), 590 mg of mono-2-(methacryloyloxy)ethyl succinate (490 μL, 2.56 mmol, 2.0 eq.), 62 mg of 4-dimethylaminopyridine (0.51 mmol, 0.4 eq.) and 1.3 g of N,N′-dicyclohexylcarbodiimide (6.40 mmol, 5 eq.) were dissolved in 20 mL of DMF and stirred at room temperature overnight. The white suspension was concentrated under reduced pressure and purified with flash column chromatography (SiO_2, ethyl acetate/hexane 1:1 to 4:1) to isolate the product as a colorless oil (800 mg, 1.03 mmol, 81 % yield). ^{1}H NMR (Fig. S4, Bruker 400 MHz in MeOD): δ (ppm) Methacrylic protons: 6.12 (s, 1H, C(=O)–C(-CH$_3$)═C*H*H), 5.58 (s, 1H, C(=O)–C(-CH$_3$)═CH*H*), 1.93 (s, 3H, C(=O)–C(-C*H*$_3$)═CH$_2$); DEX A-ring protons: 7.21 (d, 1H), 6.31 (dd, 1H), 6.08 (d, 1H); Linking protons: 4.89–5.06 (dd, 2H, DEX-C*H*$_2$-O-C(=O)–CH$_2$–CH$_2$-MAES), 2.63–2.82 (m, 4H, DEX–CH$_2$–O-C(=O)–C*H*$_2$–C*H*$_2$-MAES). (LC-MS (ESI, +, *m/z*): found: 605 theoretical: 605.27.

2.2.5. 6-Methacrylamidohexanoic acid

6-methacrylamidohexanoic acid was adapted from a previously reported protocol [50]. 3.9 g of 6-aminocaproic acid (30 mmol) was dissolved in 3 mL of dH_2O to which 1.2 g of NaOH dissolved in 3 mL of dH_2O (30 mmol, 1 eq.) were added. After cooling to 0 °C, 2.9 mL of neat methacryloyl chloride (3.1 g, 30 mmol, 1 eq.) and a solution of 1.2 g of NaOH in 6 mL of dH_2O (30 mmol, 1 eq.) were added dropwise simultaneously over 30 min. After stirring at room temperature for 1 h, the solution was acidified with concentrated HCl to pH 2. The raw product oil was extracted with dichloromethane, dried over $MgSO_4$, and recrystallized from ethyl acetate, to yield the product as a white crystalline solid (3.5 g, 18 mmol, 60 % yield). ^{1}H NMR (Fig. S5, Bruker 400 MHz in DMSO-d_6): δ (ppm) 12.00 (s, 1H, (CH$_2$)$_5$–COO*H*), 7.88 (s, 1H, *H*N–C(=O)–C(-CH$_3$)═CH$_2$), 5.62 (s, 1H, C(=O)–C(-CH$_3$)═C*H*H), 5.29 (s, 1H, C(=O)–C(-CH$_3$)═CH*H*), 3.09 (q, 2H, NH–C*H*$_2$-(CH$_2$)$_4$–COOH), 2.20 (t, 2H, NH–(CH$_2$)$_4$–C*H*$_2$–COOH), 1.85 (s, 3H, C(=O)–C(-C*H*$_3$)═CH$_2$), 1.21–1.56 (m, 6H, NH–CH$_2$-(C*H*$_2$)$_3$–CH$_2$–COOH.

2.2.6. Dexamethasone-6-methacrylamidohexanoic acid (DEX-MAHAc)

160 mg of Dexamethasone (0.41 mmol, ABCR Karlsruhe, GER), 100 mg of 6-methacrylamidohexanoic acid (0.5 mmol, 1.2 eq.), 12 mg of 4-dimethylaminopyridine (0.10 mmol, 0.25 eq.) and 160 mg of N,N′-dicyclohexylcarbodiimide (0.78 mmol, 1.9 eq.) were dissolved in 2 mL of DMF and stirred at room temperature overnight. The white suspension was concentrated under reduced pressure and purified with flash column chromatography (SiO_2, ethyl acetate/hexane 2:1 to pure ethyl acetate) to isolate the product as a colorless oil (178 mg, 0.31 mmol, 76 % yield). ^{1}H NMR (Fig. S6, Bruker 400 MHz in MeOD): δ (ppm) Methacrylic protons: 5.67 (s, 1H, C(=O)–C(-CH$_3$)═C*H*H), 5.31 (s, 1H, C(=O)–C(-CH$_3$)═CH*H*), 1.93 (s, 3H, C(=O)–C(-C*H*$_3$)═CH$_2$); DEX A-ring

protons: 7.23 (d, 1H), 6.33 (dd, 1H), 6.11 (d, 1H); Linking protons: 4.82–5.04 (dd, 2H, DEX-CH_2-O-C(=O)–CH_2-MAHAc), 2.31–2.50 (m, 2H, DEX–CH_2–O-C(=O)–CH_2-MAHAc). (LC-MS (ESI, +, *m/z*): found: 575 theoretical: 574.31.

2.3. Polymer preparation and purification

2.3.1. Free radical polymerization (FRP)

See below a representative protocol for the synthesis of a fluorescently labelled pCBAA homopolymer via FRP. Other (co)polymers were synthesized analogously by changing the main monomer or adding comonomers to the reaction feed including 2-methacryloyloxyethyl phosphorylcholine (PCMA), *N*-(2- hydroxypropyl)methacrylamide (HPMA) and (3-acrylamidopropyl)trimethylammonium (APTAC).

820 mg of CBAA (3.6 mmol), 1.17 mg of acryloxyethyl thiocarbamoyl rhodamine B (1.8 μmol, 0.05 mol%) and 4.5 mg of V-65 (18 μmol, 0.5 mol%, WAKO Fujifilm, Düsseldorf, GER) were dissolved in 4 mL of trifluoroethanol. After purging with N_2 for 10 min, the solutions were stirred under protection from light at 55 °C overnight. The conversion of the polymerization was estimated via ^{1}H NMR by comparing the integrals at δ 5.87 ppm and 3.66 ppm. The reaction mixture was diluted with dH_2O, transferred to seamless cellulose dialysis membranes (12.4 kDa MWCO), dialyzed against 0.1 M NaCl (3 × 12h) and dH_2O (3 × 12h) and lyophilized to yield the purified polymer as a pink, fluffy solid (605 mg, 74 % yield).

2.3.2. Reversible addition-fragmentation-transfer polymerization (RAFT)

See below a representative protocol for the synthesis of a fluorescently labelled pCBAA homopolymer via RAFT polymerization. The polymerization of PCMA proceeded analogously, however, using 4-cyano-4-[(dodecylsulphanylthiocarbonyl)sulfanyl] pentanoic acid as the chain transfer agent.

144 mg of CBAA (634 μmol), 0.21 mg of acryloxyethyl thiocarbamoyl rhodamine B (0.32 μmol, 0.05 mol%) and 0.31 mg of V-65 (1.27 μmol, 0.2 mol%) were dissolved in 700 μL of trifluoroethanol. After purging with N_2 for 10 min, the solutions were stirred under protection from light at 55 °C overnight. The conversion of the polymerization was estimated via ^{1}H NMR by comparing the integrals at δ 5.87 ppm and 3.66 ppm. The reaction mixture was diluted with dH_2O, transferred to regenerated cellulose dialysis membranes (3.4 kDa MWCO, Spectrum Laboratories, Auckland, New Zealand), dialyzed against 0.1 M NaCl (3 × 12h) and dH_2O (3 × 12h) and lyophilized to yield the purified polymer as a pink, fluffy solid (112 mg, 78 % yield).

2.4. Size exclusion chromatography (SEC)

Polymers were dissolved at 2 mg/mL in a 4:1 v/v mixture of 0.05 M Trizma pH 7.4, 0.2 M NaNO3 with acetonitrile. SEC analysis was performed on an Agilent 1260 Infinity II system (Agilent technologies, Santa Clara, USA) at a flow rate of 1 mL/min and over two PL-Aquagel-OH MIXED-M columns (Agilent technologies, Santa Clara, USA). The molecular weight distribution was calculated from the refractive index detector by comparison with a series of polyethylene glycol standards (Agilent technologies, Santa Clara, USA).

2.5. Release kinetics

1 mg/mL polymer solutions were prepared in 1x PBS at pH 5.0, 7.4 and 9.8 as well as in Fluorobrite DMEM (Thermo Fisher Scientific, Waltham, USA) and kept under standard cell culture conditions (37 °C, 5 % CO_2, 95 % humidity). DEX release at any given time was quantified with HPLC analysis on a Hitachi Chromaster system (Hitachi, Chiyoda, JPN) equipped with a Poroshell 120 CS-C18 column (Agilent technologies, Santa Clara, USA) by integrating the dexamethasone peak(s) in the 240 nm spectrum. Note that DEX-MAES-containing polymers showed two peaks in the chromatograms due to the increased number of linking esters compared to DEX-MAHAc, which only had one ester.

2.6. Acid/base titration

Solutions of CBAA, pCBAA and pPCMA in dH_2O were prepared at a matching functional group molarity of 25 mM and titrated with 1 M NaOH and 1 M HCl respectively. pH changes were measured with an FE20 pH meter (Mettler Toledo, Columbus, USA). pKa values were determined with the Henderson-Hasselbalch equation.

2.7. Electrophoretic mobility

Electrophoretic mobility and Zeta potential of polymers (10 mg/mL in dH_2O) was measured on a Zetasizer Nano device (Malvern Panalytical, Malvern, USA). Every sample was measured three times with each measurement consisting of an averaged 10 reads.

2.8. Cartilage explant experiments

2.8.1. Culture medium

Bovine cartilage explants were cultured in DMEM + GlutaMAX medium (high glucose, pyruvate, Thermo Fisher Scientific, Waltham, USA) supplemented with 1x ITS (Thermo Fisher Scientific, Waltham, USA) and 10 μg/mL Gentamycin.

2.8.2. Bovine cartilage explant harvesting and culture

Cartilage explants were harvested from bovine elbow joints obtained from the local slaughterhouse (Angst AG, Zurich, CH) from freshly slaughtered 1-to-2-year-old cows and immediately processed. The cartilage was peeled off the medial condyle using a low-profile microtome blade (Sakura Finetek, Umkirch, GER) and washed in sterile 1x PBS supplemented with 1x Antibiotic-Antimycotic (Thermo Fisher Scientific, Waltham, USA) for 2 h with several changes of the wash solution. Using biopsy punchers (KAI MEDICAL, Seki, JPN), cartilage disks of the desired size were prepared and placed with the superficial zone facing up in cell culture well plates fitted with silicone (SYLGARD 184, Dow Chemical, Midland, USA) fixtures (Fig. 7a). For the next 7 days, they were left to recover from the harvesting in culture medium under standard cell culture conditions (37 °C, 5 % CO_2, 95 % humidity) before being used for subsequent experiments. The thickness of harvested cartilage explant disks ranged between 400 and 800 μm with an average of 550 μm.

2.8.3. Chondroprotection studies

Explants were first treated with polymers, polymer-drug conjugates, or free DEX for 24 h, washed three times with culture medium and then cultured for up to 3 weeks in culture medium supplemented with 10 ng/mL human IL-1β (PeproTech, London, United Kingdom). Explants were cultured under gentle agitation (60 rpm) on an orbital shaker, and the medium was replenished every 2–3 days. Media was collected and stored at −20 °C for later biochemical analysis. After 2 and 3 weeks respectively, disks were washed with 1x PBS and halved. One half was fixed in 4 % formaldehyde and prepared for histology and the other was kept in culture to evaluate GAG synthesis rates (only for 3-week timepoint).

2.8.4. Cell viability studies

Explants were treated with polymers, polymer-drug conjugates, or free DEX for 1 or 4 days, washed three times with 1x PBS and incubated with Calcein-AM and Hoechst 33342 in Fluorobrite DMEM (all from Thermo Fisher Scientific, Waltham, USA) for 30 min, washed three times with Fluorobrite DMEM and then kept in Fluorobrite DMEM. The articular surface of the explants was imaged on a Leica SP8 confocal microscope (Leica Microsystems GmBH, Wetzlar, GER) and viability calculated as the fraction of Calcein-AM- to Hoechst-positive cells in two regions per disk with an average of 50 cells per analyzed region.

2.9. Biochemical analysis

2.9.1. sGAG quantification in culture medium

sGAG release into culture medium was quantified with the Blyscan™ sGAG assay kit (Biocolor, Carrickfergus, UK) following the instructions of the supplier. Media was diluted 1:1 with culture medium prior to analysis.

2.9.2. Nitric oxide quantification in culture medium

Release of NO into culture medium was quantified using the Griess Reagent Kit (Invitrogen, Waltham, USA) following the instructions of the supplier. A Synergy H1 plate reader (BioTek, Winooski, USA) was used to read the absorbance at 548 nm.

2.9.3. Metabolic activity assay

After being treated with different sample solutions, explants were washed three times with culture medium and 2.5 % v/v MTS reagent (Abcam, Cambridge, UK) in culture medium was added to each well. After 40 min, 100 µL of medium was transferred to a separate plate and the absorbance at 490 nm read on a Synergy H1 plate reader (BioTek, Winooski, USA). Metabolic activity was calculated relative to the absorbance of untreated (100 %) and 70 % EtOH treated (0 %) explants.

2.9.4. GAG synthesis assay

Cartilage explants were cultured in medium supplemented with 10 µCi/mL $Na^{35}SO_4$ (Hartmann Analytic, Braunschweig, GER) for 3 h. Explants were washed thoroughly with three changes of PBS over 2 h under gentle agitation (60 rpm) to wash out any unbound $Na^{35}SO_4$ and subsequently dissociated in 200 µL of 4:1 v/v Soluene-350:isopropanol at 60 °C and under vigorous agitation (1000 rpm) for 2 h. Homogenized samples were diluted 10-fold in OptiPhase HiSafe 3 liquid scintillation cocktail (Perkin Elmer, Waltham, USA) and ^{35}S-incorporation rates measured on a 2450 Microbeta2 liquid scintillator (Perkin Elmer, Waltham, USA). GAG synthesis rates were calculated relative to the untreated control.

2.10. Histology

Fixed samples were dehydrated by submersion in a series of different ethanol/water mixtures (20, 40, 60 and 70 % ethanol content, 30 min each), followed by automated paraffinization on a Milestone Logos J device (Milestone, Sorisole, ITA). After embedding in paraffin blocks, 5 µm thick longitudinal sections were prepared using a microtome (HM 325, Microm, Walldorf, GER). The sections were rehydrated with a series of washes ranging from xylene over ethanol/water mixtures with decreasing ethanol content to finally pure water. Sections were then incubated with Weigert's iron hematoxylin for 5 min, washed in dH_2O (3 × 30s), submerged in 1 % acid alcohol (2s), washed in dH_2O (3 × 30s), stained in 0.02 % fast green (1 min), destained in 1 % acetic acid (30s) and stained in 0.1 % safranin O (30 min). After washing in 95 % ethanol (3 × 30s), dehydration in 100 % ethanol (2 × 1 min), clearing in xylene (2 × 1 min) and air-drying, the sections were coverslipped using Eukitt mounting medium and the stained tissues imaged on a Pannoramic 250 Flash II slide scanner (3DHistech, Budapest, HUN). For the analysis of GAG retention levels, Safranin O staining intensity was calculated after color deconvolution using Fiji ImageJ v1.51n.

2.11. Penetration/retention testing

Untreated/IL-1β pre-treated cartilage explants were placed in custom-made silicone (SYLGARD 184, Dow Chemical, Midland, USA) penetration devices (see Fig. 2), superficial zone facing up, and 10 µL of polymer solution (10 mg/mL in 1x PBS) were added on top of the disks. The devices were wrapped in a damp tissue, put into closed petri dishes, and incubated at 37 °C for 24 h. After 24 h of penetration, the disks were briefly washed with 1x PBS, transferred into 2 mL Eppendorf tubes with 1.5 mL of 1x PBS and washed in horizontal orientation under gentle agitation (60 rpm) until termination of the experiment. At different

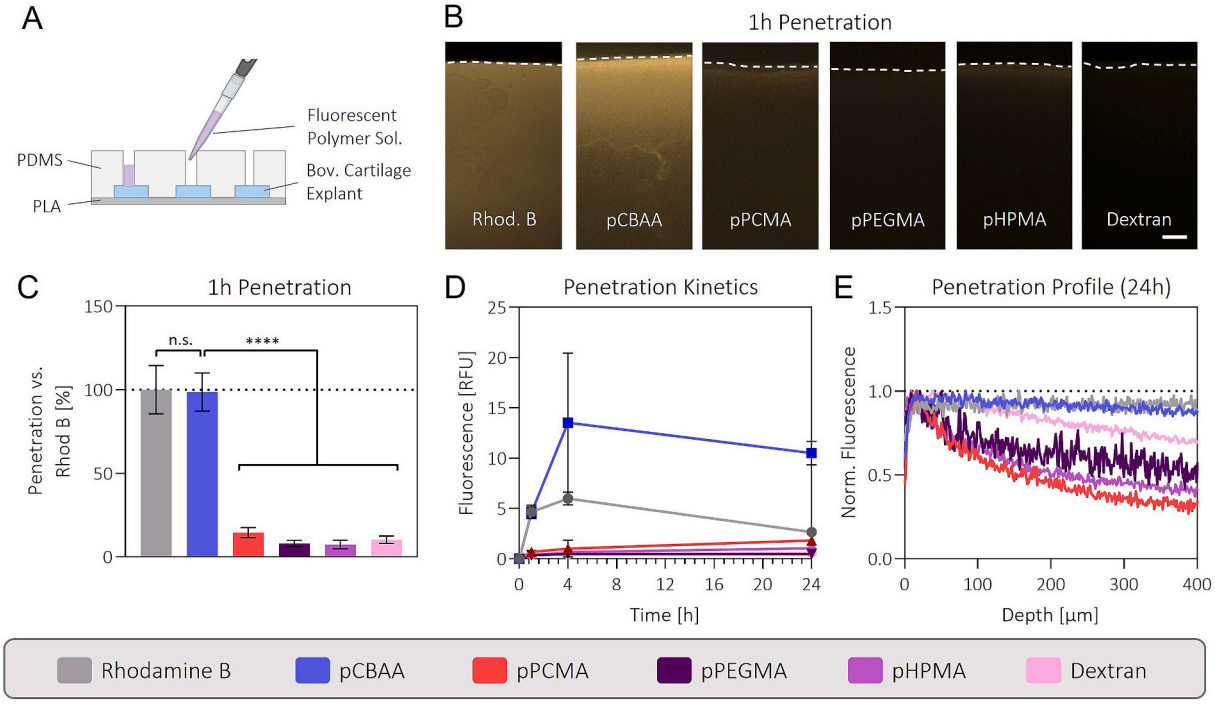

Fig. 2. pCBAA rapidly penetrates full thickness cartilage: A) Custom PDMS fixtures allow for controlled incubation of the top surface of cartilage with polymer solutions. B) Fluorescence micrographs of cartilage cross-sections showing full thickness cartilage penetration of pCBAA after 1 h of incubation. Scale bar: 100 µm. C) Quantified polymer penetration levels after 1 h, normalized to rhodamine B. Statistical analysis using one-way ANOVA with a Tukey's multiple comparisons test (non-significant (n.s.), ****$p < 0.0001$). N = 2. D) Net polymer penetration kinetics showing continued pCBAA uptake until 4 h. E) Penetration profile of polymers after 24 h showing even distribution of pCBAA throughout the cartilage tissue.

timepoints, disks were halved, and their cross-sections imaged on an epifluorescence microscope (Axio Observer.Z1, Zeiss, Oberkochen, GER). Note that since this is a destructive method, each timepoint was recorded on different tissues. Polymer penetration/retention was quantified by integrating pixel intensities from the cartilage surface down to a depth of 500 μm. To correct for small differences in fluorescence intensities of the applied sample solutions, integrated values were normalized to the fluorescence intensity reads measured on a Synergy H1 plate reader (BioTek, Winooski, USA).

2.12. Retention testing under shear and compression

4 and 5 mm cartilage explant disks were incubated with sample solutions as described in the previous section. After 24 h of penetration, the disks were glued (Cyanolit 401x, Panacol-Elosol, Steinbach, Germany) onto custom made pins, superficial zone facing up, and mounted onto an MCR 301 rheometer (5 mm on the top, 4 mm on the bottom, Anton Paar, Graz, Austria). 10 μL of equine synovial fluid was applied to lubricate the cartilage surfaces and prevent drying of the disks. The disks were first equilibrated at 10 N (=0.8 MPa) for 2 min before the top cartilage sample was rotated at a constant speed of 30 rpm for 10 min. This procedure was repeated every 24 h, with the samples incubating in culture medium at 37 °C under gentle agitation (60 rpm) in the meantime. At regular intervals, some explants were removed, and polymer retention levels calculated as in the previous section.

2.13. Compression testing

Bulk compressive moduli of bovine cartilage explants were determined on a TA.XTplus device (Stable Micro Systems, UK) with a 5 N load cell. Explants were compressed up to 20 % strain at a strain rate of 2.5 %/sec and the bulk compressive modulus calculated from the slope in the linear range between 10 and 20 % strain.

2.14. Calculation of polymer partition coefficients

4 mm cartilage explants were treated with 100 μL (V_{sol}) polymer solutions for 24 h and the fluorescence intensity of the polymer solutions recorded before (F_{before}) and after (F_{after}) the 24-h incubation period on a Synergy H1 plate reader (BioTek, Winooski, USA). By measuring the thickness of the disks with an epifluorescence microscope (Axio Observer.Z1, Zeiss, Oberkochen, GER), the explant volume V_{expl} was calculated, which allowed for calculation of the polymer partition coefficients into cartilage tissue with the below formula:

$$P_{coeff} = \frac{(F_{before} - F_{after})V_{sol}}{F_{after}V_{expl}}$$

3. Results and discussion

3.1. pCBAA polymers penetrate into cartilage explants

As for all following experiments, the polymer penetration kinetics were assessed using bovine articular cartilage explants. To ensure that the fluorescently labelled polymers were only able to enter the tissue from the top through the superficial zone, we designed a custom PDMS fixture in which cartilage disks could be held in place (Fig. 2a). To compare penetration kinetics of our zwitterionic pCBAA and pPCMA with conventional materials for drug delivery, this experiment also included poly(polyethylene glycol methacrylate) (pPEGMA), pHPMA and dextran, all of which are hydrophilic, uncharged polymers.

After 1 h, pCBAA already showed full thickness cartilage penetration with a net uptake that was greatly increased compared to any of the other investigated polymers (Fig. 2b/c). The total fluorescence in the explant was even on similar levels to the one treated with rhodamine B – a small molecule with an almost 200-fold lower molecular weight. While rhodamine B reached its equilibrium after 1 h, pCBAA continued to penetrate, nearly tripling its net uptake at the 4-h timepoint (Fig. 2d). Beyond 4 h, there was no further change in net uptake and at 24 h, pCBAA showed an even distribution across the entire cartilage depth indicating equilibrium (Fig. 2e). All other polymers were mostly surface localized with net uptake levels of 17 % and less with respect to pCBAA, indicating very slow and non-equilibrium penetration after 24 h (Fig. S7).

Due to their non-fouling properties, it was expected that the ZI polymers would show increased cartilage penetration in this experiment. The vast difference between pCBAA and pPCMA however was unexpected. Though pCBAA is generally known to be slightly more hydrated [51] and thus more non-fouling than pPCMA [52], these minor differences are insufficient to explain their disparate penetration ability. Another possible explanation is the difference in molecular weight (Mw), as the pPCMA polymers (277 kDa) were around triple the size of pCBAA (92 kDa, Table S1). Employing reversible addition fragmentation chain transfer (RAFT) polymerization, pPCMA polymers of comparable Mw to the pCBAA were synthesized without any substantial improvements in their cartilage penetration (Fig. S8). Similarly, reducing the Mw of pCBAA polymers with RAFT polymerization led to no additional improvements in penetration speed (Fig. S9). To further understand the interaction of pCBAA with cartilage tissue, we measured the partition coefficient P_{coeff} – i.e. the ratio of intra- and extra-cartilage polymer concentrations – for these polymers (Fig. S10). The value for pCBAA at 3 mg/mL was at around 40, which is in between the values of avidin ($P_{coeff} \sim 30$) [53] and chitosan ($P_{coeff} > 100$) [54], two carriers with very high affinity to cartilage due to their cationic nature. Electrophoretic mobility and zeta potential measurements then showed that pCBAA polymers also had a net positive charge, whereas pPCMA was confirmed to be neutral (Fig. 3a, Fig. S11). Comparison with pPCMA copolymerized with the cationic APTAC monomer indicated that pCBAA roughly behaves like pPCMA with 10 mol% of APTAC. This corresponds to a charge density of around 0.33 kDa^{-1}, which puts it right in between avidin (0.09 kDa^{-1}) [53] and chitosan (>0.4 kDa^{-1}) [54] and is therefore in line with the calculated partition coefficient.

Unlike phosphobetaine polymers whose anionic and cationic moieties are both completely ionized across the entire pH range, the terminal carboxylic acid in carboxybetaines can lead to some net positive charge under acidic conditions. Though most of the studies investigating the behavior of carboxybetaine polymers across different pH ranges indicate absence of charge at neutral pH [55–61], there are also two studies reporting a net positive charge [62,63]. Acid/base titration of our own polymers and monomers showed that whereas the permanently ionized pPCMA has no buffering capacity and the CBAA monomer buffers solely around its reported pKa of 3.3 [64], the pCBAA polymer has two distinct buffering ranges at pH 4.1 and 9.8 thereby indicating incomplete deprotonation at pH 7.4 (Fig. 3b). As the second range only appears for the pCBAA polymer but not the CBAA monomer, this can only be a consequence of the macromolecular architecture. We hypothesize that as the polymer gets increasingly deprotonated, the remaining protons form hydrogen bonds between two adjacent carboxylic acids, thereby greatly increasing their pKa (Fig. 3c).

To our knowledge, this is the first report suggesting such a two-step deprotonation mechanism for carboxybetaine polymers. From previous studies, we know that small changes in the molecular structure of the employed carboxybetaine monomer can lead to substantial differences in pH sensitivity [55–58]. Further in-depth characterizations will be necessary to determine whether this is a property unique to our specific pCBAA structure or whether it also translates to other members of the carboxybetaine family.

3.2. pCBAA polymers retain in healthy and GAG-depleted cartilage explants

In healthy cartilage, pure ionic interactions should anchor any

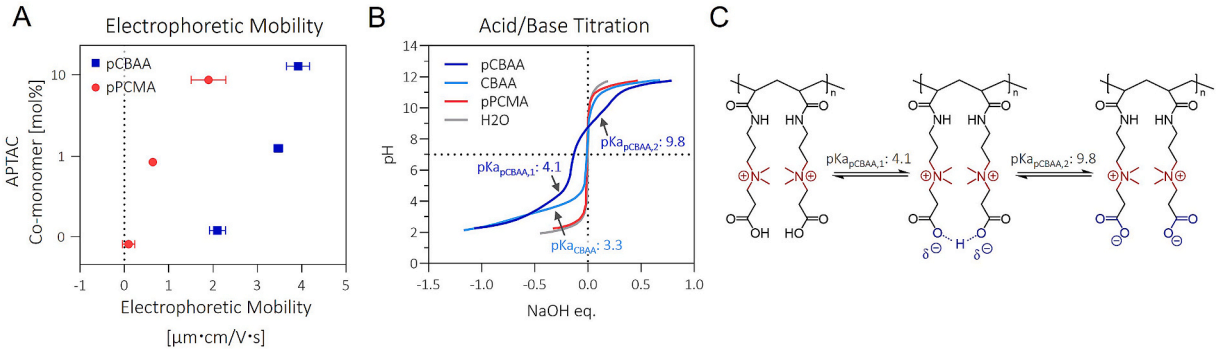

Fig. 3. pCBAA is partially protonated at physiological pH: A) Comparison of electrophoretic mobility shows that pCBAA is positively charged and behaves similarly to a pPCMA copolymer with 10 mol% cationic APTAC. B) Acid/base titration reveals two distinct regions of buffering for the pCBAA polymer whereas the CBAA monomer only displays buffering capacity in the acidic range. C) Proposed molecular mechanism to explain the observations in B).

cationic drug carrier in the ECM. In diseased cartilage, collagenases and aggrecanases however break down the ECM, which results in a loss of anionic GAGs and decreased electrostatic driving force [38]. To simulate this condition, we cultured bovine cartilage explants for two weeks in the presence of the pro-inflammatory cytokine interleukin-1 beta (IL-1β). This led to the depletion of GAGs in the superficial and middle zones of the cartilage, which is representative of patients in early-to mid-stage OA (Fig. 4a) [65]. To compensate for the decreased electrostatic interactions in GAG-depleted cartilage, we investigated three different targeting comonomers: The cationic APTAC, the collagen II-binding hexapeptide WYRGRL (C2Pep) [47] and the non-specific binder dopamine methacrylamide (DMA) [48], all of which were copolymerized with CBAA at 10 mol% (Table S1).

Analysis after 24 h of penetration indicated some correlations of the local polymer distribution with the zonal GAG differences in the GAG-depleted samples (Fig. 4a–c). Both pCBAA and pCBAA-co-C2Pep showed decreased concentration in the superficial and middle zones where the Safranin O staining indicated absence of GAGs. Conversely, in the healthy samples, both polymers were evenly distributed throughout the whole cartilage tissue. This finding indicates that for pCBAA-co-C2Pep, the electrostatic interactions are still the dominant targeting mechanism, even in GAG-depleted cartilage. Interestingly, these zonal differences cannot be observed for the pCBAA-co-APTAC polymer which showed an even distribution across all zones. This indicates that the additional cationic charges on the polymer were able to compensate for the decreased anionic charges in the tissue, thereby restoring the original levels of polymer-tissue affinity. It is important to note that even without these additional cationic charges, the uptake of pCBAA in the GAG-depleted zones still reached 75 % of the uptake in the GAG-rich deeper zones, despite the Safranin O staining indicating near binary differences in GAG-concentrations between these two regions. This suggests a very strong multivalent binding mechanism sensitive to even the smallest amounts of GAGs [66]. For pCBAA-co-DMA we observed preferred surface localization for both the healthy and GAG-depleted samples. This was generally expected as the DMA comonomer forms strong non-specific hydrogen bonds with proteins and thus gets immobilized rather quickly when entering a tissue [67].

Despite differences in local polymer distributions between the different tissue states, this did not cause any significant differences in overall net polymer uptake for any of the polymers (Fig. S12). Regarding the different targeting moieties, pCBAA-co-APTAC showed a small but statistically nonsignificant increase in net uptake compared to all other polymers, which further supports electrostatic interactions as the most effective targeting mechanism.

To evaluate polymer retention, the cartilage explants were submerged in PBS and incubated on an orbital shaker for washing. While the majority of the poorly penetrating pPCMA polymer was released from the cartilage tissue within the first 24 h, a slow but steady release was observed for all pCBAA conditions in this two-week experiment (Fig. S13). After two weeks, pCBAA, pCBAA-co-APTAC and pCBAA-co-C2Pep all still showed >50 % polymer retention, independent of the tissue state, whereas pCBAA-co-DMA retention dropped to 38 % for both tissue states. As the pCBAA-co-DMA is mostly surface localized, it makes sense that this polymer might be more susceptible to being washed away. We observed across all conditions that the polymer concentration at the cartilage surface dropped more quickly during washing than in the deeper zones (Fig. S14). It is difficult to estimate how these retention kinetics would translate to a clinical setting but based on preliminary data indicating equivalent retention kinetics under compression and shear (Fig. S15), the release should not be dramatically accelerated.

As none of the additional targeting moieties led to any significant improvements in polymer retention even in GAG-depleted tissue, we decided to use unmodified pCBAA as the basis to synthesize the polymer-drug conjugates.

3.3. *pCBAA-co-DEX conjugates show slow-release kinetics*

To incorporate DEX into our polymers, two new comonomers were synthesized, both linking the terminal carboxylic acid of a polymerizable monomer to the 21-hydroxyl group of DEX via Steglich esterification. Whereas DEX-MAES contained three esters between DEX and the methacrylate group, DEX-MAHAc only contained one ester (Fig. 5a). Both monomers were copolymerized into pCBAA polymers at >90 % conversion with the effective degrees of substitution (4.0 mol% and 5.0 mol%, Table S1) close to the feed ratio (5 mol%), indicating good compatibility of the two monomers with CBAA.

The release kinetics were determined using HPLC in DMEM culture medium at pH 7.4 and in PBS at three different pHs: 5.0, 7.4 and 9.8 (Fig. 5b). In PBS, we observed that DEX release was generally faster at increased pH, which is in line with previous studies [68,69]. Moreover, release from the pCBAA-co-DEX-MAES containing three esters was significantly faster than from pCBAA-co-DEX-MAHAc. In addition to the increased probability of cleavage with three esters compared to just one, the higher number of esters also increases the hydrophilicity of the linker as a whole and thus accelerates hydrolysis [69]. At pH 7.4 – which is in range of synovial fluid pH at 7.3–7.8 [70,71] – both conjugates showed slow zero-order release kinetics with a $t_{1/2}$ of 16.2 and 39.7 days for pCBAA-co-DEX-MAES and pCBAA-co-DEX-MAHAc respectively. Using DMEM instead of PBS, the $t_{1/2}$ however significantly decreased to 1.4 and 4.2 days, with the release now following first-order kinetics. By screening through different media components, these differences were attributed to the presence of sodium bicarbonate in DMEM (Fig. S16). Though it is known that carbonyl compounds can act as a catalyst for ester hydrolysis [72], further studies are necessary to prove this mechanism for our specific observation. As pPCMA and pCBAA conjugates behaved analogously with respect to the different media components

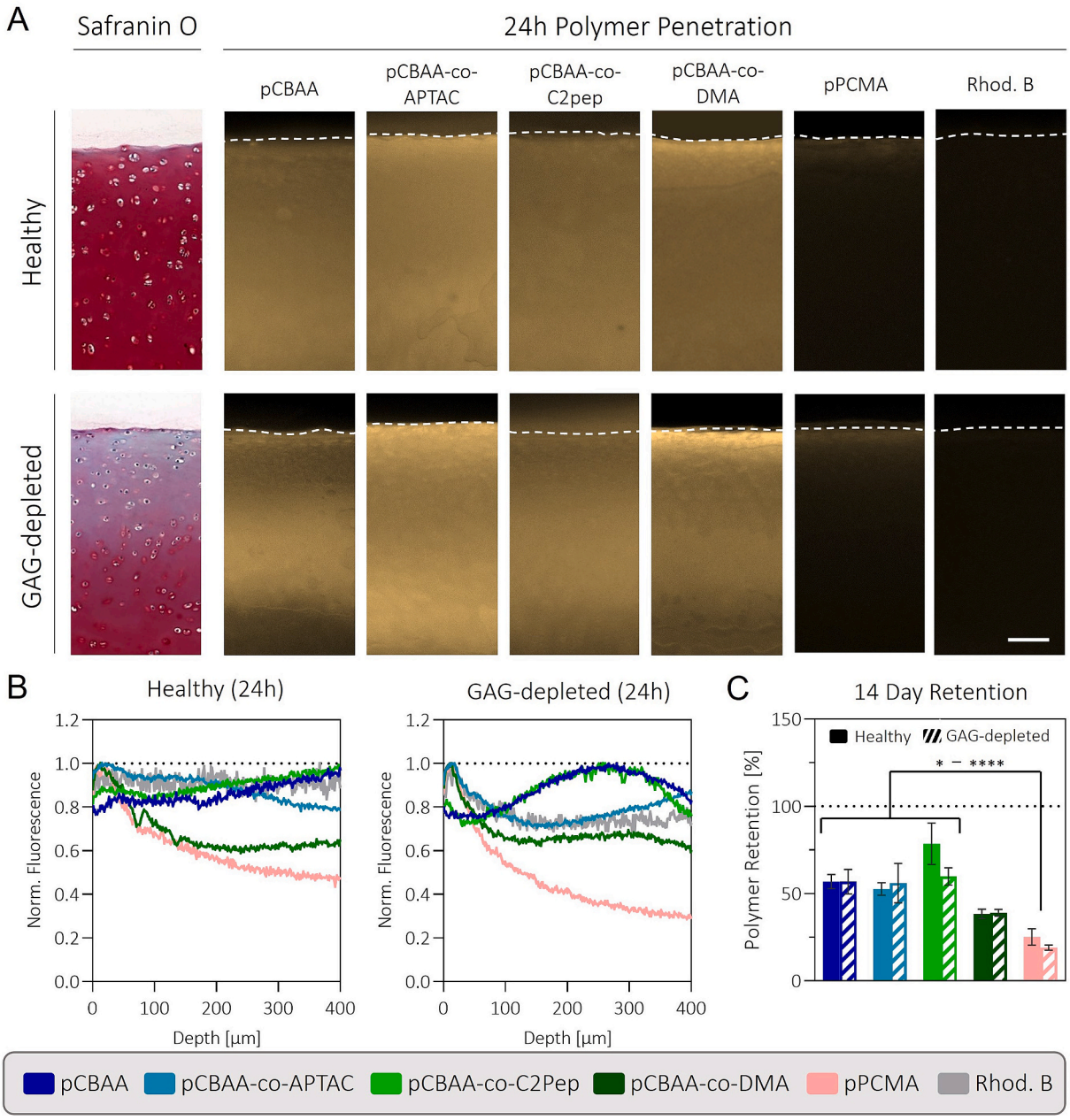

Fig. 4. pCBAA polymers penetrate and retain equally in healthy and GAG-depleted cartilage: A) Total polymer uptake after 24 h is unaffected by the depletion of GAGs in the superficial and middle zones, as seen in the Safranin O staining. Scale bar: 100 µm. B) Penetration profiles showing a more even polymer distribution in healthy compared to GAG-depleted cartilage. Introduction of the APTAC targeting moiety leads to deeper, more even penetration in GAG-depleted cartilage compared to pCBAA and pCBAA-co-C2Pep. pCBAA-co-DMA and pPCMA are equally surface-localized in both tissue states. C) Unmodified pCBAA reaches similar >50 % cartilage retention after two weeks of washing as pCBAA-co-APTAC and pCBAA-co-C2Pep. No difference between tissue states is indicated. Statistical analysis using one-way ANOVA with a Tukey's multiple comparisons test (*$p < 0.05$, ****$p < 0.0001$). N = 2.

(Fig. S16), the terminal carboxylic acids in pCBAA do not seem involved in this mechanism, implying that this effect might be more broadly applicable and could also affect hydrolytic drug release from other materials. This challenges the use of PBS as the current standard solution to determine hydrolytic drug release [26,32,34,39,73], as the pH in blood is also stabilized through carbonate buffers [74], and the determined kinetics in PBS might therefore not at all translate to subsequently performed *in vivo* experiments. Beyond passive hydrolytic release in different buffers, we also found that the addition of an esterase dose-dependently accelerates the release of DEX (Fig. S17), showing how our conjugates can also become a substrate for active enzymatic cleavage. Though the synovial fluid is known to also contain esterases [75], the concentrations are generally rather low so we expect the physiological release kinetics to be mainly driven by passive carbonate-catalyzed hydrolysis.

Despite our release kinetics in DMEM being substantially faster than in PBS, the pCBAA-co-DEX-MAHAc conjugate still shows DEX release up until day 20, underlining its slow-release properties. Comparable ester-based systems like avidin-DEX by *Bajpayee* et al. and WYRGRL-DEX by *Formica* et al. showed complete hydrolytic release already at days 4 and 6 respectively with these numbers notably being determined in PBS and not DMEM [32,39].

3.4. DEX conjugation protects chondrocytes from oxidative stress

To evaluate the biocompatibility of our conjugates, we performed a

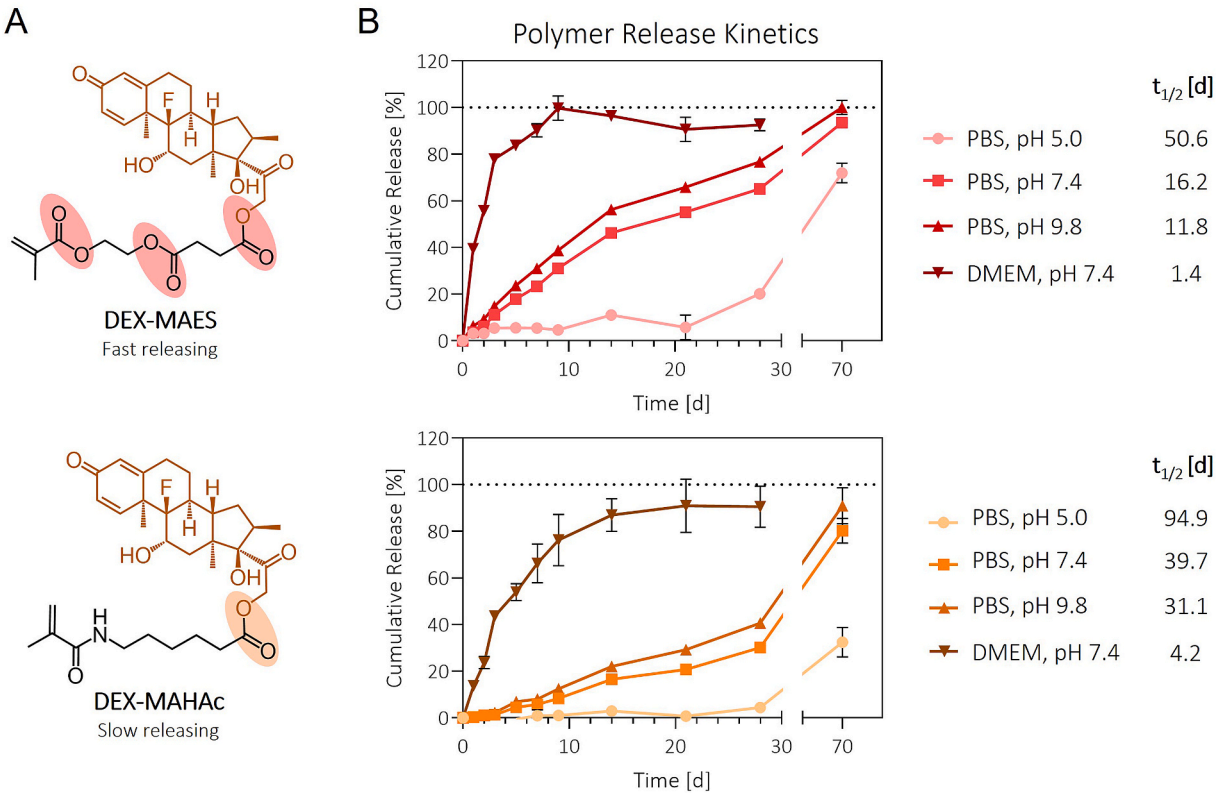

Fig. 5. Sustained drug release from pCBAA-co-DEX polymers: A) Chemical structures of the two DEX comonomers used in this study. The increased number of esters in the linker of DEX-MAES leads to faster hydrolytic release compared to DEX-MAHAc. B) pCBAA-co-DEX polymers show pH dependent, zero-order release kinetics in PBS. Dissolution in DMEM accelerates DEX release due to catalytic carbonates in the medium (Fig. S16).

series of different assays on bovine cartilage explants including the unmodified pCBAA polymer and free DEX as controls. DEX concentrations were matched between the free DEX and conjugate conditions and reached up to 2 mM, which is roughly the intraarticular concentration in patients directly after receiving an injection with the current clinical dosing [13]. After 1 and 4 days of culture, there were no noticeable changes in cell viability at the cartilage surface for any of the conditions, indicating good biocompatibility (Fig. 6a/b). As DEX has been associated with increased ROS production [17,20], generally reduced proliferation [76] and increased senescence [77] in chondrocytes, we also investigated the release of nitric oxide (NO) and metabolic activity. After both 1 h and 4 days of stimulation, 2 mM DEX triggered an increase in both NO release and metabolic activity compared to the untreated control (Fig. 6c/d). For the dose-matched polymer-drug conjugates, neither of these changes were observed after 1 h, which shows how conjugation can reduce drug bioavailability and cellular stress compared to free DEX. After 4 days of stimulation, the highest dose of either conjugate, however, triggered a decrease in metabolic activity by 90 % and 97 % (Fig. 6d). The disparate response after 1 h and 4 days can most certainly be attributed to the relatively fast release kinetics in culture medium, which after 4 days accounts for roughly 80 % and 50 % of initial drug loading for pCBAA-co-DEX-MAES and pCBAA-co-DEX-MAHAc respectively. Due to the high levels of cartilage uptake for these conjugates, the intra-tissue concentration of free DEX most probably even exceeded 2 mM at the 4-day timepoint. It remains unclear why these explants showed such a different response compared to the 2 mM free DEX condition. As there was also a small but statistically nonsignificant decrease in metabolic activity at day 4 for the highest concentration of pCBAA alone (Fig. 6d), we hypothesize that the observed effects might be a combination of the high intra-tissue concentrations of both DEX and pCBAA. It is known that at high concentrations, polycationic polymers can destabilize the cellular membrane [78], which has been associated with findings of decreased metabolic activity [79] and even cell death in cartilage [35]. Finally, we also investigated whether the treatment with pCBAA polymers affected the bulk mechanical properties of the cartilage explants and found no noticeable differences in compressive moduli (Fig. S18).

3.5. *pCBAA-co-DEX conjugates protect cartilage from inflammation*

To investigate the ability of our polymer-drug conjugates to protect cartilage from inflammation, we stimulated polymer-treated cartilage explants with the pro-inflammatory cytokine IL-1β (Fig. 7a). To mimic the orientation and inflammatory exposure of a biological joint, the cartilage explants were held by a PDMS fixture at the bottom of the well-plate with the superficial zone facing upwards. Explants were first treated with the different polymers/free DEX for 24 h before being exposed to IL-1β for 3 weeks. The conjugates were applied at 0.1 mg/mL with an effective DEX concentration of 20 μM. This dose was chosen based on its good biocompatibility, with the goal of reducing the amount of required polymer carrier as much as possible while maintaining good solubility, and for the fact that it would – based on the cartilage partition coefficients and the determined release kinetics for pCBAA-co-DEX-MAHAc – sustain media concentrations of DEX above 100 nM for the entire duration of the experiment.

We analyzed the levels of GAG-depletion at weeks 2 and 3 with histology and found that the only conditions showing statistically significant protective effects compared to the IL-1β control were the two conjugates pCBAA-co-DEX-MAES (at week 3) and pCBAA-co-DEX-MAHAc (at weeks 2 & 3, Fig. 7b/c, Fig. S19). In accordance with the expected release kinetics over this period, the slow-release pCBAA-co-DEX-MAHAc conjugate allowed for increased GAG protection compared to the fast-release pCBAA-co-DEX-MAES, albeit without statistical significance. Contrary to our expectation, not only free DEX but also

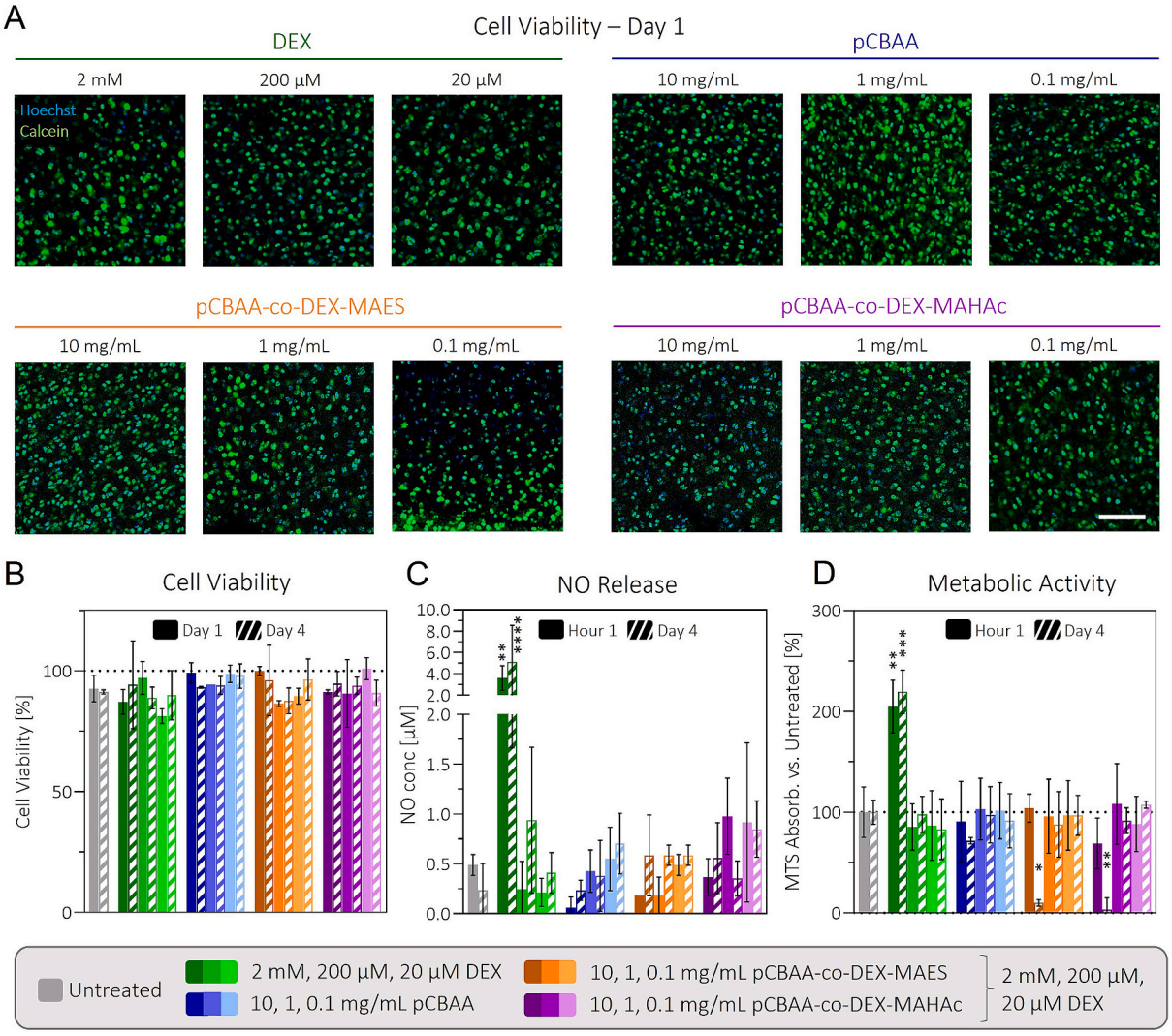

Fig. 6. Polymer conjugation protects chondrocytes from oxidative stress of free DEX: A) Fluorescence micrographs indicating preserved cell viability in cartilage explants after 24h of incubation with polymer-drug conjugates/pCBAA/free DEX. Scale bar: 100 µm. B) Quantified cell viability at days 1 and 4. C/D) Stimulation of explants with a clinical dose of free DEX for 1 h or 4 days increases the release of nitric oxides to the medium (C) and general metabolic activity (D). Dose-matched polymer-drug conjugates show no increased NO release but decreased metabolic activity at the highest dose. Statistical analysis using one-way ANOVA with a Tukey's multiple comparisons test. Significance is indicated with respect to the untreated control. (*$p < 0.05$, **$p < 0.01$, ***$p < 0.001$, ****$p < 0.0001$). N = 3.

pCBAA alone offered some level of protection from inflammation. This effect is currently under investigation in a separate study, but it seems that the increased therapeutic efficacy of the conjugates compared to free DEX might be due not only to the sustained release kinetics but also to the chemical and physical properties of the pCBAA material itself.

To better understand the differences seen in histology, we investigated NO and soluble GAG (sGAG) release into the media as well as GAG synthesis rates. For both NO and sGAG assays, the IL-1β control showed the strongest response (vs. untreated) on day 2 with NO and sGAG concentrations then continuously decreasing over time (Fig. S20). At day 2, all treatments equally decreased the NO and sGAG concentrations compared to the IL-1β control by around 70 % and 60 % respectively. Beyond day 2, however, we no longer observed any significant treatment effects. Regarding GAG synthesis, we found that at week 3, the conjugate-treated explants displayed significantly increased synthesis rates compared to the IL-1β control. Whereas the conjugate-treated explants retained 37 % of untreated synthesis levels, the IL-1β control retained almost no ability to synthesize GAGs (3 %, Fig. 7d). For the free DEX and pCBAA conditions, GAG synthesis rates were also increased compared to the IL-1β control, although at lower levels compared to the conjugates. Taken together, these findings indicate that the superiority of the polymer-drug conjugates in the histology compared to the other treatments is a consequence of improved protection of the anabolic pathways, while the catabolic pathways are downregulated equally across all tested treatments.

4. Conclusion

We have synthesized a modular polymeric drug delivery system based on pCBAA with excellent cartilage penetration and retention kinetics both in healthy and GAG-depleted tissue. Through titration studies, we discovered that pCBAA carries some net positive charge at physiological pH, which attracts these polymers to the negatively charged cartilage ECM and enables tissue retention over more than 2 weeks. By incorporating DEX-coupled comonomers, we created polymer-drug conjugates with sustained release kinetics which after application to cartilage explants decreased the production of NO compared to dose-matched free DEX, indicating the reduced bioavailability upon conjugation. Finally, a single dose of conjugates protected cartilage explants from inflammation by decreasing the release of GAGs

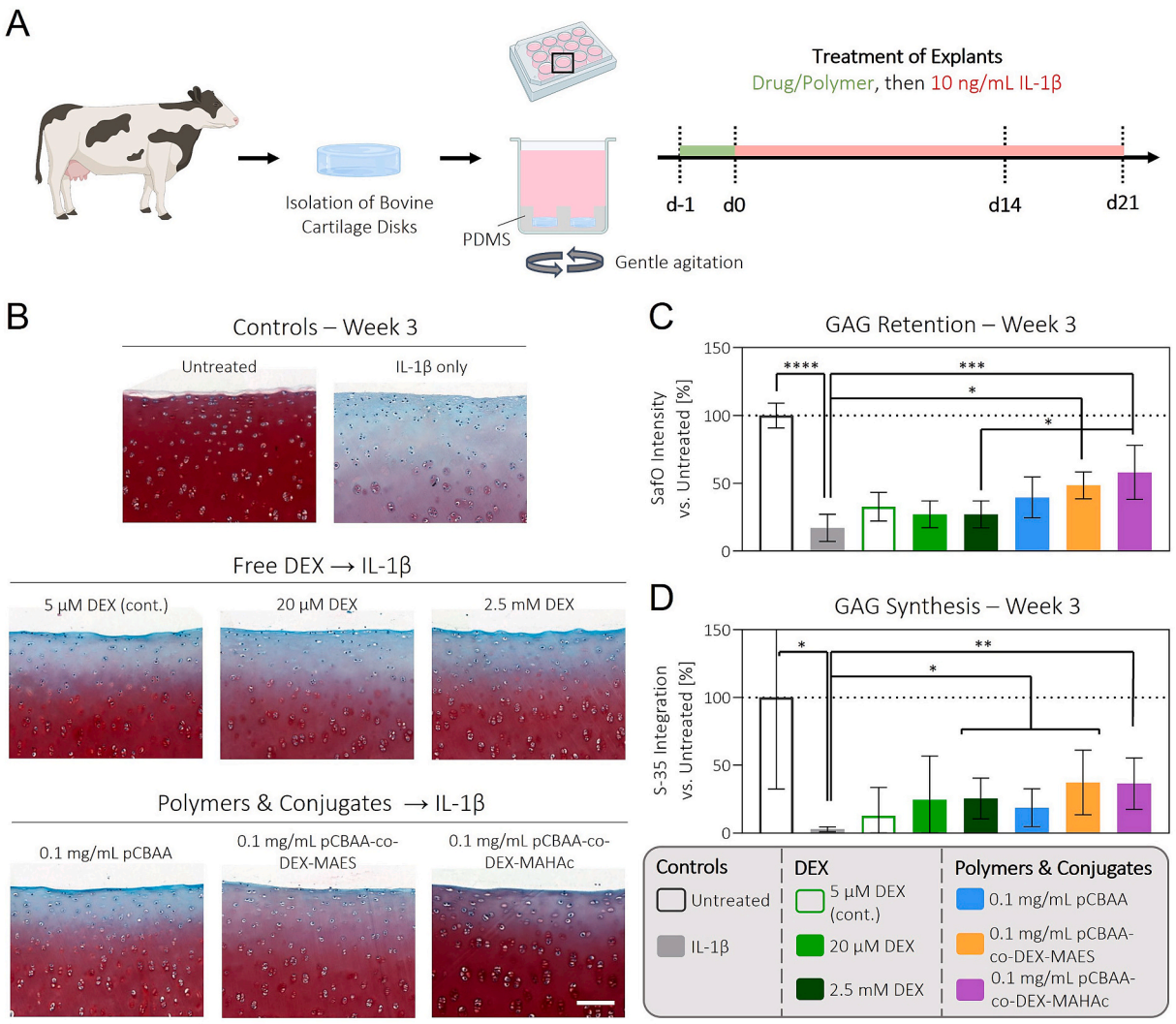

Fig. 7. Polymer-drug conjugates protect cartilage from IL-1β-induced inflammation: A) Fixation of bovine cartilage explants in PDMS molds in a well plate ensures physiological one-sided exposure of tissue to polymers and IL-1β during the 3-week experiment. B) Safranin O staining of cartilage explants showing chondroprotective effects of free DEX and pCBAA which are further improved when combined in pCBAA-co-DEX conjugates. Scale bar: 100 μm C) Quantified Safranin O staining intensity. D) GAG synthesis rates after 3 weeks measured by integration of radioactive ^{35}S. Statistical analysis using one-way ANOVA with a Tukey's multiple comparisons test (*$p < 0.05$, **$p < 0.01$, ***$p < 0.001$, ****$p < 0.0001$). N = 6.

and production of NO in the acute phase and preserving GAG synthesis rates in the long term.

Ultimately, *in vitro* experiments are conducted in a strongly controlled environment which can only reproduce a small part of this highly complex disease. Therefore, the full therapeutic potential of our polymer-drug conjugates can only be assessed once they have been tested in an animal model of OA. Nevertheless, we are convinced that the use of more specific and controllable drug delivery vehicles is the key to achieving better clinical outcomes when treating joint disease, and we hope that our modular pCBAA conjugates can make a substantial contribution in the future.

Funding

This work was supported by the Swiss National Science Foundation (Grant No. 315230_192656 to MZW).

CRediT authorship contribution statement

Patrick Weber: Writing – review & editing, Writing – original draft, Visualization, Validation, Project administration, Methodology, Investigation, Formal analysis, Data curation, Conceptualization. **Maryam Asadikorayem:** Writing – review & editing, Methodology, Investigation, Conceptualization. **František Surman:** Writing – review & editing, Supervision, Funding acquisition, Conceptualization. **Marcy Zenobi-Wong:** Writing – review & editing, Methodology, Funding acquisition, Conceptualization.

Declaration of competing interest

The authors declare the following financial interests/personal relationships which may be considered as potential competing interests: Marcy Zenobi-Wong reports financial support was provided by Swiss National Science Foundation. If there are other authors, they declare that they have no known competing financial interests or personal relationships that could have appeared to influence the work reported in this paper.

Data availability

Our data is available at the ETH research collection

Acknowledgements

We would like to thank Dr. Marina Fonti and Annalena Maier from our lab for their support with the histology and the peptide synthesis respectively. We also thank the ScopeM center at ETH Zurich for providing technical support with microscopy and histological processing.

Appendix A. Supplementary data

Supplementary data to this article can be found online at https://doi.org/10.1016/j.mtbio.2024.101049.

References

[1] J. Fuchs, R. Kuhnert, C. Scheidt-Nave, 12-month prevalence of osteoarthritis in Germany, J. Health Monit. 2 (3) (2017) 51 [Online]. Available: https://www.ncbi.nlm.nih.gov/pmc/articles/PMC10165920/. (Accessed 30 October 2023).

[2] L.R. Soma, C.E. Uboh, Y. You, F. Guan, R.C. Boston, Pharmacokinetics of intra-articular, intravenous, and intramuscular administration of triamcinolone acetonide and its effect on endogenous plasma hydrocortisone and cortisone concentrations in horses, Am. J. Vet. Res. 72 (9) (Sep. 2011) 1234–1242, https://doi.org/10.2460/ajvr.72.9.1234.

[3] C. Larsen, et al., Intra-articular depot formulation principles: Role in the management of postoperative pain and arthritic disorders, J. Pharm. Sci. 97 (11) (2008) 4622–4654, https://doi.org/10.1002/jps.21346.

[4] T. Brown, U. Laurent, F. Jr, Turnover of hyaluronan in synovial joints: elimination of labelled hyaluronan from the knee joint of the rabbit, Exp. Physiol. 76 (1) (1991) 125–134, https://doi.org/10.1113/expphysiol.1991.sp003474.

[5] U. Lindqvist, V. Tolmachev, K. Kairemo, G. Åström, E. Jonsson, H. Lundqvist, Elimination of Stabilised hyaluronan from the knee joint in healthy men, Clin. Pharmacokinet. 41 (8) (Jul. 2002) 603–613, https://doi.org/10.2165/00003088-200241080-00004.

[6] A. Stout, J. Friedly, C.J. Standaert, Systemic absorption and side effects of locally injected glucocorticoids, PM&R 11 (4) (2019) 409–419, https://doi.org/10.1002/pmrj.12042.

[7] J.L. Hollander, The local effects of compound F (hydrocortisone) injected into joints, Bull. Rheum. Dis. 2 (2) (Oct. 1951) 3–4.

[8] S. Stone, G.A. Malanga, T. Capella, Corticosteroids: review of the history, the effectiveness, and adverse effects in the treatment of joint pain, Pain Physician 24 (S1) (2021) S233 [Online]. Available: https://www.njregenerativeinstitute.com/system/resources/W1siZiIsIjIwMjEvMDEvMjYvMTcvNDMvMTkvNjgyMGYzNDMtZjk5Yi00NGM1LTgyYmEtZDQ1ZGRiNjhmNzlhL0NvcnRpY29zdGVyb2lkIFJldmlldyBQYWluIFBoeXNpY2lhbjIwMjE7MjQ7UzIzMy1TMjQ2LnBkZiJdXQ/Corticosteroid%20Review%20Pain%20Physician2021%3B24%3BS233-S246.pdf. (Accessed 23 October 2023).

[9] R.R. Bannuru, et al., OARSI guidelines for the non-surgical management of knee, hip, and polyarticular osteoarthritis, Osteoarthritis Cartilage 27 (11) (Nov. 2019) 1578–1589, https://doi.org/10.1016/j.joca.2019.06.011.

[10] American Academy of Orthopaedic Surgeons, Management of osteoarthritis of the knee (non-arthroplasty) - evidence-based clinical practice guideline, Published 08/31/2021 (2021). https://www.aaos.org/oak3cpg.

[11] S.L. Kolasinski, et al., 2019 American college of rheumatology/arthritis foundation guideline for the management of osteoarthritis of the hand, hip, and knee, Arthritis Rheumatol. 72 (2) (2020) 220–233, https://doi.org/10.1002/art.41142.

[12] R. Black, A.J. Grodzinsky, DEXAMETHASONE: chondroprotective corticosteroid or catabolic killer? Eur. Cell. Mater. 38 (Nov. 2019) 246–263, https://doi.org/10.22203/eCM.v038a17.

[13] C. Wernecke, H.J. Braun, J.L. Dragoo, The effect of intra-articular corticosteroids on articular cartilage: a systematic review, Orthop. J. Sports Med. 3 (5) (2015) 2325967115581163.

[14] H.A. Ibad, et al., Longitudinal MRI-defined cartilage loss and radiographic joint space narrowing following intra-articular corticosteroid injection for knee osteoarthritis: a systematic review and meta-analysis, Osteoarthr. Imaging 3 (3) (Sep. 2023) 100157, https://doi.org/10.1016/j.ostima.2023.100157.

[15] T.E. McAlindon, et al., Effect of intra-articular triamcinolone vs saline on knee cartilage volume and pain in patients with knee osteoarthritis: a randomized clinical trial, JAMA 317 (19) (May 2017) 1967–1975, https://doi.org/10.1001/jama.2017.5283.

[16] F. Zaman, et al., Dexamethasone differentially regulates Bcl-2 family proteins in human proliferative chondrocytes: role of pro-apoptotic Bid, Toxicol. Lett. 224 (2) (Jan. 2014) 196–200, https://doi.org/10.1016/j.toxlet.2013.10.020.

[17] N. Liu, W. Wang, Z. Zhao, T. Zhang, Y. Song, Autophagy in human articular chondrocytes is cytoprotective following glucocorticoid stimulation, Mol. Med. Rep. 9 (6) (Jun. 2014) 2166–2172, https://doi.org/10.3892/mmr.2014.2102.

[18] Y.W. Song, T. Zhang, W.B. Wang, Gluococorticoid could influence extracellular matrix synthesis through Sox9 via p38 MAPK pathway, Rheumatol. Int. 32 (11) (Nov. 2012) 3669–3673, https://doi.org/10.1007/s00296-011-2091-8.

[19] D.W. Richardson, G.R. Dodge, Dose-dependent effects of corticosteroids on the expression of matrix-related genes in normal and cytokine-treated articular chondrocytes, Inflamm. Res. 52 (1) (Jan. 2003) 39–49, https://doi.org/10.1007/s000110300012.

[20] C. Shen, G.-Q. Cai, J.-P. Peng, X.-D. Chen, Autophagy protects chondrocytes from glucocorticoids-induced apoptosis via ROS/Akt/FOXO3 signaling, Osteoarthritis Cartilage 23 (12) (Dec. 2015) 2279–2287, https://doi.org/10.1016/j.joca.2015.06.020.

[21] Y.C. Lu, C.H. Evans, A.J. Grodzinsky, Effects of short-term glucocorticoid treatment on changes in cartilage matrix degradation and chondrocyte gene expression induced by mechanical injury and inflammatory cytokines, Arthritis Res. Ther. 13 (5) (Sep. 2011) R142, https://doi.org/10.1186/ar3456.

[22] Y. Li, et al., Effects of insulin-like growth factor-1 and dexamethasone on cytokine-challenged cartilage: relevance to post-traumatic osteoarthritis, Osteoarthritis Cartilage 23 (2) (Feb. 2015) 266–274, https://doi.org/10.1016/j.joca.2014.11.006.

[23] P.S. Davies, S.M. Graham, R.J. MacFarlane, A. Leonidou, A. Mantalaris, E. Tsiridis, Disease-modifying osteoarthritis drugs: in vitro and in vivo data on the development of DMOADs under investigation, Expert Opin. Investig. Drugs 22 (4) (Apr. 2013) 423–441, https://doi.org/10.1517/13543784.2013.770837.

[24] M.A. Karsdal, et al., Disease-modifying treatments for osteoarthritis (DMOADs) of the knee and hip: lessons learned from failures and opportunities for the future, Osteoarthritis Cartilage 24 (12) (Dec. 2016) 2013–2021, https://doi.org/10.1016/j.joca.2016.07.017.

[25] Y. Han, et al., Biomimetic injectable hydrogel microspheres with enhanced lubrication and controllable drug release for the treatment of osteoarthritis, Bioact. Mater. 6 (10) (Oct. 2021) 3596–3607, https://doi.org/10.1016/j.bioactmat.2021.03.022.

[26] M.L. Kang, J.-Y. Ko, J.E. Kim, G.-I. Im, Intra-articular delivery of kartogenin-conjugated chitosan nano/microparticles for cartilage regeneration, Biomaterials 35 (37) (Dec. 2014) 9984–9994, https://doi.org/10.1016/j.biomaterials.2014.08.042.

[27] P. Maudens, S. Meyer, C. Alexander Seemayer, O. Jordan, E. Allémann, Self-assembled thermoresponsive nanostructures of hyaluronic acid conjugates for osteoarthritis therapy, Nanoscale 10 (4) (2018) 1845–1854, https://doi.org/10.1039/C7NR07614B.

[28] Y. Zhao, et al., Drug delivery system based on near-infrared light-responsive molybdenum disulfide nanosheets controls the high-efficiency release of dexamethasone to inhibit inflammation and treat osteoarthritis, ACS Appl. Mater. Interfaces 11 (12) (Mar. 2019) 11587–11601, https://doi.org/10.1021/acsami.8b20372.

[29] A. Petit, et al., Sustained intra-articular release of celecoxib from in situ forming gels made of acetyl-capped PCLA-PEG-PCLA triblock copolymers in horses, Biomaterials 53 (Jun. 2015) 426–436, https://doi.org/10.1016/j.biomaterials.2015.02.109.

[30] X. Ji, et al., Glucosamine sulphate-loaded distearoyl phosphocholine liposomes for osteoarthritis treatment: combination of sustained drug release and improved lubrication, Biomater. Sci. 7 (7) (2019) 2716–2728, https://doi.org/10.1039/C9BM00201D.

[31] I. Elron-Gross, Y. Glucksam, R. Margalit, Liposomal dexamethasone–diclofenac combinations for local osteoarthritis treatment, Int. J. Pharm. 376 (1) (Jul. 2009) 84–91, https://doi.org/10.1016/j.ijpharm.2009.04.025.

[32] F.A. Formica, G. Barreto, M. Zenobi-Wong, Cartilage-targeting dexamethasone prodrugs increase the efficacy of dexamethasone, J. Controlled Release 295 (Feb. 2019) 118–129, https://doi.org/10.1016/j.jconrel.2018.12.025.

[33] A. Homma, et al., Synthesis and optimization of hyaluronic acid–methotrexate conjugates to maximize benefit in the treatment of osteoarthritis, Bioorg. Med. Chem. 18 (3) (Feb. 2010) 1062–1075, https://doi.org/10.1016/j.bmc.2009.12.053.

[34] G. Zhao, et al., Thermoresponsive polymeric dexamethasone prodrug for arthritis pain, J. Controlled Release 339 (Nov. 2021) 484–497, https://doi.org/10.1016/j.jconrel.2021.10.007.

[35] B.C. Geiger, S. Wang, R.F. Padera, A.J. Grodzinsky, P.T. Hammond, Cartilage-penetrating nanocarriers improve delivery and efficacy of growth factor treatment of osteoarthritis, Sci. Transl. Med. 10 (469) (Nov. 2018), https://doi.org/10.1126/scitranslmed.aat8800.

[36] J. Pradal, P. Maudens, C. Gabay, C.A. Seemayer, O. Jordan, E. Allémann, Effect of particle size on the biodistribution of nano- and microparticles following intra-articular injection in mice, Int. J. Pharm. 498 (1) (Feb. 2016) 119–129, https://doi.org/10.1016/j.ijpharm.2015.12.015.

[37] S. Mehta, T. He, A.G. Bajpayee, Recent advances in targeted drug delivery for treatment of osteoarthritis, Curr. Opin. Rheumatol. 33 (1) (Jan. 2021) 94–109, https://doi.org/10.1097/BOR.0000000000000761.

[38] A.G. Bajpayee, A.J. Grodzinsky, Cartilage-targeting drug delivery: can electrostatic interactions help? Nat. Rev. Rheumatol. 13 (3) (2017) 3.

[39] A.G. Bajpayee, M.A. Quadir, P.T. Hammond, A.J. Grodzinsky, Charge based intra-cartilage delivery of single dose dexamethasone using Avidin nano-carriers suppresses cytokine-induced catabolism long term, Osteoarthritis Cartilage 24 (1) (Jan. 2016) 71–81, https://doi.org/10.1016/j.joca.2015.07.010.

[40] A.G. Bajpayee, et al., Sustained intra-cartilage delivery of low dose dexamethasone using a cationic carrier for treatment of post traumatic osteoarthritis, Eur. Cell. Mater. 34 (Dec. 2017) 341–364, https://doi.org/10.22203/eCM.v034a21.

[41] C. Rodriguez Emmenegger, E. Brynda, T. Riedel, Z. Sedlakova, M. Houska, A. B. Alles, Interaction of blood plasma with antifouling surfaces, Langmuir 25 (11) (Jun. 2009) 6328–6333, https://doi.org/10.1021/la900083s.

[42] L. Zhang, et al., Zwitterionic hydrogels implanted in mice resist the foreign-body reaction, Nat. Biotechnol. 31 (6) (2013) 6.

[43] S. Mai, et al., Carboxybetaine-based zwitterionic polymer nanogels with long blood circulation for cancer therapy, Biomacromolecules 24 (5) (May 2023) 2392–2405, https://doi.org/10.1021/acs.biomac.3c00247.

[44] W. Lin, et al., Biocompatible long-circulating star carboxybetaine polymers, J. Mater. Chem. B 3 (3) (2015) 440–448, https://doi.org/10.1039/C4TB01477D.
[45] S. Fujii, S. Takano, K. Nakazawa, K. Sakurai, Impact of zwitterionic polymers on the tumor permeability of molecular bottlebrush-based nanoparticles, Biomacromolecules (Apr. 2022), https://doi.org/10.1021/acs.biomac.2c00216.
[46] Y. Zhang, W. Chen, C. Yang, Q. Fan, W. Wu, X. Jiang, Enhancing tumor penetration and targeting using size-minimized and zwitterionic nanomedicines, J. Controlled Release 237 (Sep. 2016) 115–124, https://doi.org/10.1016/j.jconrel.2016.07.011.
[47] D.A. Rothenfluh, H. Bermudez, C.P. O'Neil, J.A. Hubbell, Biofunctional polymer nanoparticles for intra-articular targeting and retention in cartilage, Nat. Mater. 7 (3) (Mar. 2008) 248–254, https://doi.org/10.1038/nmat2116.
[48] H. Lee, B.P. Lee, P.B. Messersmith, A reversible wet/dry adhesive inspired by mussels and geckos, Nature 448 (7151) (Jul. 2007) 7151, https://doi.org/10.1038/nature05968.
[49] C. Rodriguez-Emmenegger, et al., Substrate-independent approach for the generation of functional protein resistant surfaces, Biomacromolecules 12 (4) (Apr. 2011) 1058–1066, https://doi.org/10.1021/bm101406m.
[50] J. Drobník, et al., Enzymatic cleavage of side chains of synthetic water-soluble polymers, Makromol. Chem. 177 (10) (1976) 2833–2848, https://doi.org/10.1002/macp.1976.021771003.
[51] W. Zhao, et al., A comprehensive study and comparison of four types of zwitterionic hydrogels, J. Mater. Sci. 53 (19) (Oct. 2018) 13813–13825, https://doi.org/10.1007/s10853-018-2535-6.
[52] Y. Liu, et al., Molecular simulations and understanding of antifouling zwitterionic polymer brushes, J. Mater. Chem. B 8 (17) (2020) 3814–3828, https://doi.org/10.1039/D0TB00520G.
[53] A.G. Bajpayee, C.R. Wong, M.G. Bawendi, E.H. Frank, A.J. Grodzinsky, Avidin as a model for charge driven transport into cartilage and drug delivery for treating early stage post-traumatic osteoarthritis, Biomaterials 35 (1) (Jan. 2014) 538–549, https://doi.org/10.1016/j.biomaterials.2013.09.091.
[54] B. Sterner, M. Harms, S. Wöll, M. Weigandt, M. Windbergs, C.M. Lehr, The effect of polymer size and charge of molecules on permeation through synovial membrane and accumulation in hyaline articular cartilage, Eur. J. Pharm. Biopharm. 101 (Apr. 2016) 126–136, https://doi.org/10.1016/j.ejpb.2016.02.004.
[55] Sk A. Ali, Aal-e-Ali, Synthesis and solution properties of a quaternary ammonium polyelectrolyte and its corresponding polyampholyte, Polymer 42 (19) (Sep. 2001) 7961–7970, https://doi.org/10.1016/S0032-3861(01)00289-0.
[56] J. Bohrisch, O. Grosche, U. Wendler, W. Jaeger, H. Engelhardt, Electroosmotic mobility and aggregation phenomena of model polymers with permanent cationic groups, Macromol. Chem. Phys. 201 (4) (2000) 447–452, https://doi.org/10.1002/(SICI)1521-3935(20000201)201:4<447::AID-MACP447>3.0.CO;2-0.
[57] J. Bohrisch, T. Schimmel, H. Engelhardt, W. Jaeger, Charge interaction of synthetic polycarboxybetaines in bulk and solution, Macromolecules 35 (10) (May 2002) 4143–4149, https://doi.org/10.1021/ma0122019.
[58] V.A. Izumrudov, N.I. Domashenko, M.V. Zhiryakova, O.V. Davydova, Interpolyelectrolyte reactions in solutions of polycarboxybetaines, 2: influence of alkyl spacer in the betaine moieties on complexing with polyanions, J. Phys. Chem. B 109 (37) (Sep. 2005) 17391–17399, https://doi.org/10.1021/jp0518207.
[59] D.-J. Liaw, C.-C. Huang, Dilute solution properties of poly(3-dimethyl acryloyloxyethyl ammonium propiolactone), Polymer 38 (26) (Jan. 1997) 6355–6362, https://doi.org/10.1016/S0032-3861(97)00211-5.
[60] V. Neagu, S. Vasiliu, S. Racovita, Adsorption studies of some inorganic and organic salts on new zwitterionic ion exchangers with carboxybetaine moieties, Chem. Eng. J. 162 (3) (Sep. 2010) 965–973, https://doi.org/10.1016/j.cej.2010.07.002.
[61] D.B. Thomas, Y.A. Vasilieva, R.S. Armentrout, C.L. McCormick, Synthesis, characterization, and aqueous solution behavior of electrolyte- and pH-responsive carboxybetaine-containing cyclocopolymers, Macromolecules 36 (26) (Dec. 2003) 9710–9715, https://doi.org/10.1021/ma0345807.
[62] A. Niu, D.-J. Liaw, H.-C. Sang, C. Wu, Light-scattering study of a zwitterionic polycarboxybetaine in aqueous solution, Macromolecules 33 (9) (May 2000) 3492–3494, https://doi.org/10.1021/ma991622b.
[63] S. Hladysh, et al., Comparison of carboxybetaine with sulfobetaine polyaspartamides: nonfouling properties, hydrophilicity, cytotoxicity and model nanogelation in an inverse miniemulsion, J. Appl. Polym. Sci. 139 (19) (2022) 52099, https://doi.org/10.1002/app.52099.
[64] J.G. Weers, et al., Effect of the intramolecular charge separation distance on the solution properties of betaines and sulfobetaines, Langmuir 7 (5) (1991) 854–867.
[65] C. Pauli, et al., Comparison of cartilage histopathology assessment systems on human knee joints at all stages of osteoarthritis development, Osteoarthritis Cartilage 20 (6) (Jun. 2012) 476–485, https://doi.org/10.1016/j.joca.2011.12.018.
[66] C. Fasting, et al., Multivalency as a chemical organization and action principle, Angew. Chem. Int. Ed. 51 (42) (2012) 10472–10498, https://doi.org/10.1002/anie.201201114.
[67] N. Bandara, H. Zeng, J. Wu, Marine mussel adhesion: biochemistry, mechanisms, and biomimetics, J. Adhes. Sci. Technol. 27 (18–19) (Oct. 2013) 2139–2162, https://doi.org/10.1080/01694243.2012.697703.
[68] M.D. Howard, A. Ponta, A. Eckman, M. Jay, Y. Bae, Polymer micelles with hydrazone-ester dual linkers for tunable release of dexamethasone, Pharm. Res. (N. Y.) 28 (10) (Oct. 2011) 2435–2446, https://doi.org/10.1007/s11095-011-0470-1.
[69] A.E. Rydholm, K.S. Anseth, C.N. Bowman, Effects of neighboring sulfides and pH on ester hydrolysis in thiol–acrylate photopolymers, Acta Biomater. 3 (4) (Jul. 2007) 449–455, https://doi.org/10.1016/j.actbio.2006.12.001.
[70] M.D. Roman, et al., Assesment of synovial fluid pH in osteoarthritis of the HIP and knee, Rev Chim 68 (6) (2017) 1242–1244 [Online]. Available: https://www.academia.edu/download/66940501/19_20ROMAN_20M_206_2017.pdf. (Accessed 23 October 2023).
[71] I. Milošev, V. Levašič, J. Vidmar, S. Kovač, R. Trebše, pH and metal concentration of synovial fluid of osteoarthritic joints and joints with metal replacements, J. Biomed. Mater. Res. B Appl. Biomater. 105 (8) (2017) 2507–2515, https://doi.org/10.1002/jbm.b.33793.
[72] K. Bowden, Intramolecular catalysis: carbonyl groups in ester hydrolysis, Chem. Soc. Rev. 24 (6) (1995) 431–435 [Online]. Available: https://pubs.rsc.org/en/content/articlepdf/1995/cs/cs9952400431. (Accessed 24 October 2023).
[73] T. He, I. Shaw, A. Vedadghavami, A.G. Bajpayee, Single-dose intra-cartilage delivery of kartogenin using a cationic multi-arm avidin nanocarrier suppresses cytokine-induced osteoarthritis-related catabolism, CARTILAGE 13 (2) (Apr. 2022) 19476035221093072, https://doi.org/10.1177/19476035221093072.
[74] N.J. Russell, G.M. Powell, J.G. Jones, P.J. Winterburn, J.M. Basford, The blood buffering systems, Croom Helm Biology in Medicine Series, in: N.J. Russell, G. M. Powell, J.G. Jones, P.J. Winterburn, J.M. Basford (Eds.), Blood Biochemistry, Springer Netherlands, Dordrecht, 1982, pp. 131–136, https://doi.org/10.1007/978-94-011-7892-1_10.
[75] I.H. Storgaard, J. Kristensen, C. Larsen, N. Mertz, J. Østergaard, S.W. Larsen, Diclofenac prodrugs for intra-articular depot injectables: in vitro hydrolysis and species variation, J. Pharm. Sci. 109 (4) (Apr. 2020) 1529–1536, https://doi.org/10.1016/j.xphs.2020.01.003.
[76] T. Mushtaq, C. Farquharson, E. Seawright, S.F. Ahmed, Glucocorticoid effects on chondrogenesis, differentiation and apoptosis in the murine ATDC5 chondrocyte cell line, J. Endocrinol. 175 (3) (Dec. 2002) 705–713, https://doi.org/10.1677/joe.0.1750705.
[77] E. Xue, Y. Zhang, B. Song, J. Xiao, Z. Shi, Effect of autophagy induced by dexamethasone on senescence in chondrocytes, Mol. Med. Rep. 14 (4) (Oct. 2016) 3037–3044, https://doi.org/10.3892/mmr.2016.5662.
[78] S. Vaidyanathan, B.G. Orr, M.M. Banaszak Holl, Role of cell membrane–vector interactions in successful gene delivery, Acc. Chem. Res. 49 (8) (Aug. 2016) 1486–1493, https://doi.org/10.1021/acs.accounts.6b00200.
[79] J. Gong, J. Nhan, J.-P. St-Pierre, E.R. Gillies, Designing polymers for cartilage uptake: effects of architecture and molar mass, J. Mater. Chem. B 11 (36) (2023) 8804–8816, https://doi.org/10.1039/D3TB01417G.